JCTC Journal of Chemical Theory and Computation

Article

pubs.acs.org/JCTC

Simulations of Pore Formation in Lipid Membranes: Reaction Coordinates, Convergence, Hysteresis, and Finite-Size Effects

Neha Awasthi* and Jochen S. Hub*

Institute for Microbiology and Genetics, Georg-August-Universität, Justus-von-Liebig Weg 11, 37077 Göttingen, Germany

ABSTRACT: Transmembrane pores play an important role in various biophysical processes such as membrane permeation, membrane fusion, and antimicrobial peptide activity. In principal, all-atom molecular dynamics (MD) simulations provide an accurate model of pore formation in lipid membranes. However, the free energy landscape of transmembrane pore formation remains poorly understood, partly because potential of mean force (PMF) calculations of pore formation strongly depend on the choice of the reaction coordinate. In this study, we used umbrella sampling to compute PMFs for pore formation using three different reaction coordinates, namely, (i) a coordinate that steers the lipids in the lateral direction away from the pore center, (ii) the distance of a single lipid phosphate group from the membrane center, and (iii) the average water density inside a membrane-spanning cylinder. Our results show that while the three reaction coordinates efficiently form pores in membranes, they suffer from strong hysteresis between pore-opening and pore-closing simulations, suggesting that they do not restrain the systems close to the transition state for pore formation. The two reaction coordinates that act via restraining the lipids lead to more pronounced hysteresis compared with the coordinate acting on the water molecules. By comparing PMFs computed from membranes with different numbers of lipids, we observed significant artifacts from the periodic boundary conditions in small simulation systems. Further analysis suggests that the formation and disruption of a continuous hydrogen-bonding network across the membrane corresponds to the transition state for pore formation. Our study provides molecular insights into the critical steps of transmembrane pore formation, and it may guide the development of efficient reaction coordinates for pore formation.

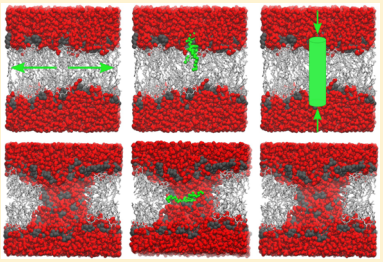

INTRODUCTION

Formation of transmembrane pores is important for many biophysical processes such as transport of small molecules and ions, cellular signaling, and membrane fusion.[1−6] In addition, formation of pores provides a mechanism to control cell death, as employed by T cells and natural killer cells to kill virus-infected cells.[7,8] Drugs derived from antimicrobial peptides act via pore-mediated pathways.[9] Likewise, cell-penetrating peptides may deliver cargos across membranes by forming defects in the lipid bilayer.[10] The mechanisms of antimicrobial and cell-penetrating peptides are far from fully understood. Thus, a quantitative understanding of the process of pore formation and pore closure may contribute to the design and control of antimicrobial and cell-penetrating peptides.

Experimentally, transmembrane pores have been investigated in detail using model systems such as vesicles. Pores were observed under various stress conditions such as surface tension, temperature, and electrochemical gradients.[11−14] Typically, experiments provide estimates of the pore size as well as rates of pore formation and closure. In parallel, molecular dynamics (MD) simulations have been used to study transmembrane pores in molecular detail.[15,16] Pores were formed in silico by applying surface tension[17,18] or electrostatic membrane potentials,[17,19−21] by simulating membrane-active agents such as antimicrobial or cell-penetrating peptides,[22−24] or by inserting small charged solutes into the membrane.[25,26] Pores were also observed as metastable intermediate structures during spontaneous aggregation of membranes.[27]

The mechanism and free-energy landscape of transmembrane pore formation are still not understood. Bennett and Tieleman[3] observed water wires prior to spontaneous pore formation in a thin dilauroylphosphatidylcholine (DLPC) membrane, but it is unclear whether a similar mechanism holds for thicker and biologically more relevant membranes. Decades ago it was suggested that a free energy barrier separates the open pore from the intact membrane, thus implying a metastable "prepore" state.[13,28,29] However, the existence of such metastable prepore states has remained controversial.[30] Likewise, only little understanding of the structures and energies of the transition state for pore formation has developed.

In principle, it should be possible to compute the free energy landscape for pore formation using MD simulations and enhanced sampling techniques such as umbrella sampling.[31] However, umbrella sampling requires the definition of one or several suitable reaction coordinates, along which the system is steered and the potentials of mean force (PMFs) are calculated. Devising such a reaction coordinate is far from trivial.[32] In the context of pore formation, the reaction coordinate should steer the system from the state of an intact membrane to the state with an open transmembrane pore. However, this criterion is not sufficient for a good reaction coordinate. Instead, steering the system along the reaction coordinate should also allow one

Received: April 12, 2016
Published: June 2, 2016

DOI: 10.1021/acs.jctc.6b00369
J. Chem. Theory Comput. 2016, 12, 3261−3269

to restrain the system close to the transition state. With such an ideal reaction coordinate, free energy calculations may converge within reasonable simulation time, and the calculations would not exhibit significant hysteresis between pore-opening and pore-closing pathways. In contrast, PMF calculations using suboptimal reaction coordinates face severe limitations: (i) they converge slowly; (ii) rate-limiting barriers may be integrated out if the barriers are oriented perpendicular (in phase space) to the reaction coordinate; and (iii) if the transition state is not sampled multiple times within a single simulation, such as one window of an umbrella sampling simulation, it is impossible to obtain a converged free energy difference between the intact membrane and the open transmembrane pore. In recent years, a number of reaction coordinates for pore formation have been suggested. Steering the simulation systems along these coordinates was found to efficiently form pores in the membranes.[33−36] However, the convergence of the PMFs computed along these coordinates have not yet been systematically compared, and it remains unclear whether the coordinates are indeed capable of restraining the systems close to the transition state.

In the present work, we tested the convergence of umbrella sampling simulations using three suggested reaction coordinates for pore formation: (i) the collective radial coordinate method proposed by Tolpekina et al.;[33] (ii) the distance of a single phosphate group from the bilayer center, as suggested by Tieleman and Marrink;[36] and (iii) the average water density inside a membrane-spanning cylinder, as suggested by Mirjalili and Feig.[35] The convergence was quantified by comparing pore-opening and pore-closing simulations and by analyzing increasing equilibration times. Our results show that all three reaction coordinates are suitable for forming pores in membranes. However, the time scale of convergence of the PMFs strongly differs among the three methods. In addition, we observed large hysteresis between pore-opening and pore-closing simulations. This finding further suggests that these reaction coordinates do not restrain the system close to the transition state for pore formation, leading to poor sampling of the transition state. On the basis of our simulations and previous ones,[3] we suggest that the transition state is characterized by the formation or rupture of a membrane-spanning continuous water channel. Hence, we suggest that future efforts should focus on the development of reaction coordinates that directly probe the presence of a *continuous* water hydrogen-bonding network.

METHODS

Reaction Coordinates for Pore Formation. In recent years, three different reaction coordinates have been proposed for modeling of transmembrane pore formation in MD simulations. These coordinates are briefly described in the following.

Reaction Coordinate 1: Collective Radial Coordinate. The first reaction coordinate we tested was proposed by Tolpekina et al.,[30,33] and we refer to it as the "collective radial coordinate" ξ_R. With this coordinate, the transmembrane pore is created by pushing all of the lipid molecules radially outward (in the *xy* plane) from the center of the pore (Figure 1A). The reaction coordinate is defined as

$$\xi_R = \frac{\Sigma - \Sigma_0}{N - \Sigma_0} \tag{1}$$

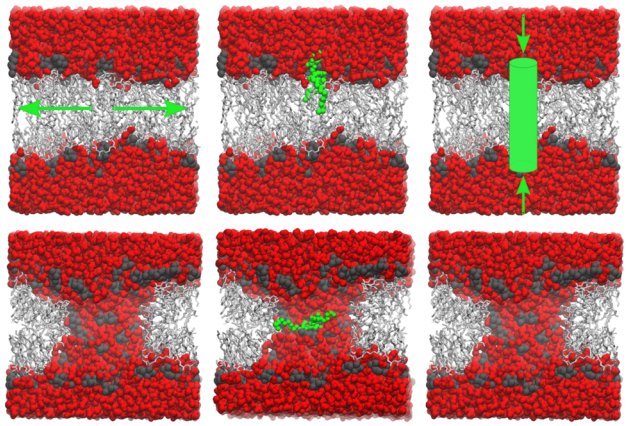

Figure 1. Illustration of the three reaction coordinates used for free energy calculation of pores. (A) Collective radial reaction coordinate.[30,33] (B) Distance of a single phosphate group from the bilayer center.[36] (C) Water density inside a membrane-spanning cylinder.[35]

in which

$$\Sigma = \sum_{i=1}^{N} \tanh(r_i/\zeta) \tag{2}$$

where N is the total number of lipid molecules and r_i is the lateral distance between the center of the pore and the center of mass of lipid i. The parameter ζ determines the approximate radius of the fully formed pore, and it was chosen as 1 nm as suggested by Tolpekina et al.[33] Σ_0 is the equilibrium value of Σ, which can be computed by assuming a random distribution of lipids. The hyperbolic tangent serves as a switch function that ensures that lipids close to the pore center are pushed more strongly in the radial direction compared with lipids that are far away from the pore. The reaction coordinate is normalized such that $\xi_R = 0$ denotes the initial state with no pore and a random distribution of lipids while $\xi_R \approx 1$ corresponds to a fully established transmembrane pore.

Reaction Coordinate 2: Distance of One Phosphate Group from the Bilayer Center. The second reaction coordinate applied in this study was suggested by Tieleman, Marrink, and co-workers[36] and is defined as the distance of a single lipid phosphate group from the membrane center, d_{ph} (Figure 1B). This reaction coordinate is mainly motivated by the observation that pulling a phosphate group to the membrane center triggers the formation of a water pore, primarily because the charged phosphate group drags water inside the membrane.

Reaction Coordinate 3: Water Density inside a Membrane-Spanning Cylinder. The third reaction coordinate considered here is defined as the average water density inside a membrane-spanning cylinder (Figure 1C), as suggested by Mirjalili and Feig.[35] Accordingly, a cylinder is defined with radius R_{cyl} and height Z_{cyl}, with the axis aligned with the bilayer normal and placed symmetrically at the membrane center. The coordinate is given by

$$\rho_V = \Gamma_V / V \tag{3}$$

where V is the volume of the cylinder and Γ_V denotes the number of water molecules inside the cylinder, calculated as

$$\Gamma_V = \sum_{i=1}^{N_w} f(\mathbf{R}_i) = \sum_{i=1}^{N_w} f_{radial}(r_i) f_{axial}(z_i) \tag{4}$$

DOI: 10.1021/acs.jctc.6b00369
J. Chem. Theory Comput. 2016, 12, 3261−3269

where N_w denotes the total number of water molecules, $\mathbf{R}_i$ is the Cartesian coordinate of water oxygen atom i, and f is an indicator function that is equal to unity inside and zero outside the cylinder. To obtain a coordinate that is differentiable with respect to the water coordinates, f is smoothly switched to zero at the cylinder boundaries using third-order polynomials.[35] For a cylinder aligned along the z axis, $f(\mathbf{R}_i)$ is given by a product of (i) a function of the radial distance r_i from the cylinder axis, $f_{\text{radial}}(r_i)$, and (ii) a function of the z coordinate of water i, $f_{\text{axial}}(z_i)$. The volume of the cylinder is $V = \int f(\mathbf{R})\, d\mathbf{R}$. It is important to note that ρ_V does not correspond to a three-dimensional density field but instead is a scalar quantity that gives the *number* of water molecules inside the cylinder.

Simulation Setup and Parameters. Membrane bilayers with 64, 128, 256, or 512 dimyristoylphosphatidylcholine (DMPC) molecules along with water molecules were constructed. The systems with 64, 128, and 256 lipids were hydrated with 40 water molecules per lipid, and the system with 512 lipids was hydrated with 48 water molecules per lipid. Each system was equilibrated until the box dimensions and the potential energy were fully converged. Parameters from Berger et al.[38] were used for DMPC, and water was modeled with the SPC model.[39] The simulations were performed with the GROMACS 4.6 simulation software.[40] The SETTLE algorithm[41] was used to constrain water bonds and angles. All of the other bonds were constrained using LINCS.[42] All of the simulations were performed at 323 K using a stochastic dynamics integrator.[43] The pressure was controlled at 1 bar using a semi-isotropic weak coupling scheme (τ = 1 ps).[44] Since the DMPC model did not contain any explicit hydrogen atoms, a time step of 4 fs was applied. Dispersive interactions and short-range repulsion were described by a Lennard-Jones potential with a cutoff at 1 nm. Electrostatic interactions were calculated using the particle-mesh Ewald method[45,46] using a 1 nm real-space cutoff and a Fourier grid spacing of 0.12 nm.

Umbrella Sampling along the Three Different Reaction Coordinates. PMFs were computed along the three reaction coordinates using a membrane of 128 lipids. In addition, in order (i) to test the effect of system size on the convergence of the PMFs and (ii) to allow direct comparison with previous studies,[30,35,37] additional PMFs using membranes of 64, 256, and 512 lipids were computed. The umbrella simulations are summarized in Table 1.

All of the PMFs for opening and closing of transmembrane pores were computed with umbrella sampling.[31] The PMFs were constructed from the umbrella histograms using the weighted histogram analysis method (WHAM) as implemented in the g_wham software.[47,48] The umbrella histograms were visually inspected to ensure sufficient overlap between adjacent histograms. All of the PMFs were defined to equal zero in the equilibrium state in the absence of any pore. The reaction coordinates ξ_R and ρ_V were implemented for umbrella sampling in an in-house modification of GROMACS 4.6.[40] Umbrella sampling simulations along d_{ph} were done with the default version of GROMACS 4.6.

Umbrella Sampling along the Collective Radial Coordinate. In order to test whether hysteresis would affect the computed PMFs, initial frames for umbrella sampling were taken from "slow-growth" pore-opening or pore-closing simulations. Accordingly, starting in the equilibrium state, the pore was opened by pulling the system along the reaction coordinate ξ_R with a harmonic potential (force constant = 50 000 kJ mol^{-1}). The minimum of the harmonic potential was moved with constant velocity from $\xi_R = 0$ at time 0 to $\xi_R = 1$ at 100 ns. Subsequently, the pore was closed by steering the system from $\xi_R = 1$ to $\xi_R = 0$ within 100 ns. Initial frames for "pore-opening" or "pore-closing" umbrella sampling simulations (see below) were taken from these opening and closing slow-growth pulling simulations. The parameter Σ_0 was computed prior to the simulations as $\Sigma_0 = \int_{\text{box}} \tanh[\zeta^{-1}((x - L/2)^2 + (y - L/2)^2)^{1/2}]\, dx\, dy$, where the integral was taken over the membrane area.

Table 1. Summary of Umbrella Sampling Simulations of Pore Formation[a]

reaction coordinate	direction	N_{lipids}	N_{win}	t_{sim} (ns)
ξ_R	pore-opening	128	40	500
ξ_R	pore-closing	128	40	500
ξ_R	pore-opening	512	40	50
ξ_R	pore-closing	512	40	50
d_{ph}	pore-opening	64	21	500
d_{ph}	pore-closing	64	21	500
d_{ph}	pore-opening	128	21	500
d_{ph}	pore-closing	128	21	1000
ρ_V	pore-opening	128	40	500
ρ_V	pore-closing	128	40	500
ρ_V	pore-opening	256	40	200
ρ_V	pore-closing	256	40	200

[a]Definitions: "direction" indicates whether starting frames were taken from pore-opening or pore-closing simulations; N_{lipids} is the number of DMPC lipids; N_{win} is the number of umbrella windows; t_{sim} is the simulation time per window.

PMFs along the collective radial coordinate ξ_R were computed for membranes of 512 and 128 DMPC lipids. Umbrella sampling was performed using 40 umbrella windows equally spaced between $\xi_R = 0$ and $\xi_R = 0.8$. An umbrella force constant of 40 000 kJ mol^{-1} was used. Each umbrella window was simulated for 50 or 500 ns for the system with 512 or 128 lipids, respectively.

The water content between pore-opening and pore-closing PMF calculations was quantified by the number of water molecules inside a membrane-spanning cylinder, N_{water}. Here N_{water} was taken as the function Γ_V defined for the water density reaction coordinate suggested by Mirjalili and Feig[35] (see eq 4) using R_{cyl} = 0.6 nm and Z_{cyl} = 3.2 nm. N_{water} was averaged within each umbrella simulation (see below). N_{water} was calculated from the 500 ns trajectory for the 128 patch and from the 50 ns trajectory for the 512 patch. Statistical errors in N_{water} were computed by binning analysis.[49]

Umbrella Sampling along the Distance of a Phosphate from the Membrane Center. The PMFs along the reaction coordinate d_{ph} were computed for membranes of 64 and 128 lipids. Initial frames for umbrella sampling were taken from slow-growth pore-opening or pore-closing simulations that steered the membrane along the d_{ph} coordinate. For the pore-opening simulation, within 50 ns the center of mass of one phosphate group was pulled from the equilibrium position ($d_{ph} \approx 1.63$ nm) to the center of the membrane ($d_{ph} = 0$) using a harmonic potential on the phosphate moving at constant velocity (force constant = 3000 kJ mol^{-1} nm^{-2}). Subsequently, the state at $d_{ph} = 0$ was equilibrated for 500 ns. Eventually, the phosphate was pulled out of the membrane within 50 ns. In addition, to obtain starting configurations for an increased distance of the phosphate from the membrane center, the same

DOI: 10.1021/acs.jctc.6b00369
J. Chem. Theory Comput. 2016, 12, 3261−3269

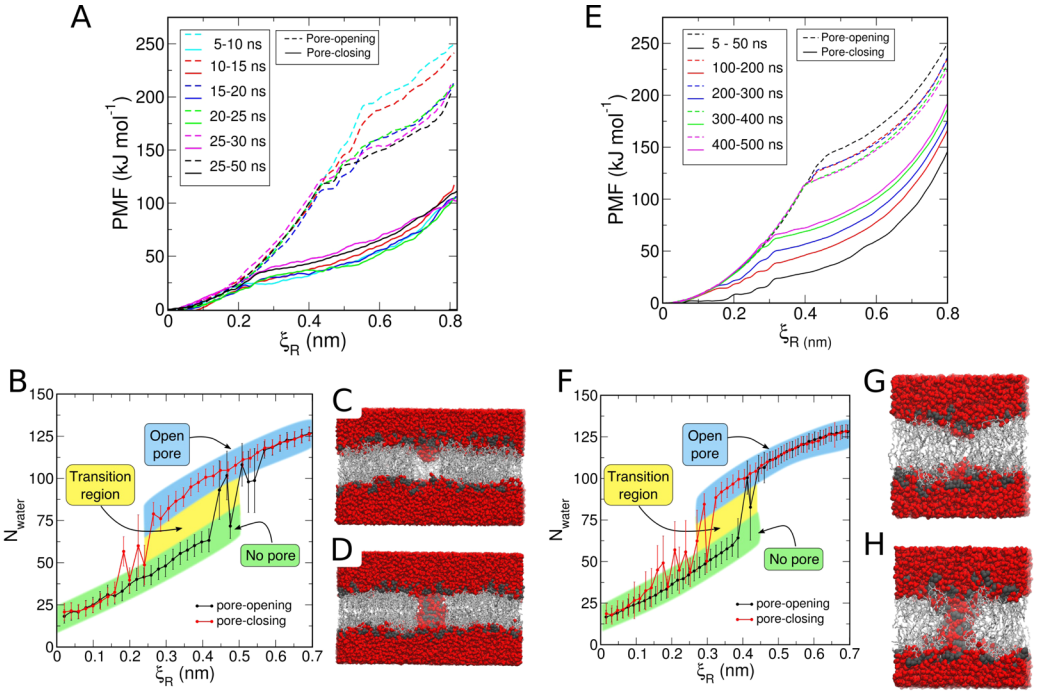

Figure 2. Pore formation using the collective radial reaction coordinate[30,33] and a membrane of (A–D) 512 or (E–H) 128 DMPC lipids. (A, E) PMFs for pore-opening (dashed lines) and pore-closing (solid lines) using an increasing equilibration time in umbrella sampling simulations (color codes are given in the legends). (B, F) Number of water molecules N_{water} in a cylindrical region around the pore as a function of ξ_R, taken from the pore-opening (black lines) or pore-closing (red lines) umbrella windows. The N_{water} curves demonstrate pronounced hysteresis. Regions with an open membrane-spanning pore (blue), without a pore (green), and the transition region between (yellow) are indicated by shaded areas. (C, G) Final umbrella simulation snapshots at $\xi_R \approx 0.37$ taken from pore-opening umbrella simulations exhibiting no open pore. (D, H) Final simulation snapshots at $\xi_R \approx 0.37$ taken from pore-closing umbrella simulations exhibiting an open pore. These snapshots demonstrate that the pore-opening and pore-closing simulations sampled different water structures. Lipid tails are visualized as gray sticks, head groups as black spheres, and water atoms as red spheres.

phosphate was pulled up to 0.38 nm toward the bulk water within 20 ns.

Umbrella sampling was performed using 21 equally spaced umbrella windows. The phosphate was restrained along the membrane normal with a harmonic umbrella potential (force constant = 3000 kJ mol^{-1} nm^{-2}). Umbrella windows for pore-closing PMFs with the 128-lipid system were simulated for 1 μs, and all other windows were simulated for 500 ns.

Umbrella Sampling along the Water Density Coordinate. PMFs along the water density coordinate were computed for membranes of 256 and 128 lipids. Initial frames for umbrella sampling were taken from slow-growth pore-opening or pore-closing simulations that steered the membrane along the Γ_V coordinate. Starting from the equilibrium state, the system was pulled up to $\Gamma_V = 125$ within 25 ns using a harmonic potential along Γ_V with a force constant of 5 kJ mol^{-1}. Next, the 256- and 128-lipid systems were restrained in the open-pore state and equilibrated for 200 and 500 ns, respectively. Subsequently, the system was pulled back to the equilibrium value of Γ_V within 25 ns.

During umbrella sampling, the system was restrained along Γ_V. The membrane-spanning cylinder was defined with R_{cyl} = 0.6 nm and Z_{cyl} = 3.2 nm. The width of the switching region in the radial direction was taken as w = 0.2 nm, and the respective width along z was taken as h = 0.6 nm.[35] Forty umbrella windows were distributed along the reaction coordinate. Umbrella potentials with a force constant of 5 kJ mol^{-1} were applied. Each umbrella simulation was conducted for 200 or 500 ns for the membrane system with 256 or 128 DMPC lipids, respectively. After the PMF was computed as a function of Γ_V, it was translated into a function of the water density relative to the density of bulk water, ρ_V/ρ_{bulk}, where ρ_{bulk} was taken as 32 water molecules nm^{-3}. Hence, $\rho_V/\rho_{bulk} = 0$ and $\rho_V/\rho_{bulk} = 1$ correspond to empty and water-filled cylinders, respectively.

RESULTS

In order to test the convergence of the PMFs along the three reaction coordinates, initial coordinates for umbrella sampling were taken from either slow-growth pore-opening simulations or slow-growth pore-closing simulations (see Methods). These PMFs are in the following called "pore-opening PMFs" or "pore-closing PMFs", respectively. Since the PMF is an equilibrium quantity, it should not depend on the initial coordinates used for PMF calculations, and consequently, the calculated pore-opening and pore-closing PMFs should be identical. In other words, any difference between pore-opening and pore-closing PMFs is indicative of poor convergence due to long autocorrelation times and hysteresis.

Collective Radial Reaction Coordinate on Lipids. Figure 2A,E shows the PMFs calculated using the collective radial reaction coordinate ξ_R for membranes of 512 and 128 lipids, respectively.[30,33] Umbrella simulations were conducted for 50 ns for the 512-lipid bilayer (Figure 2A) and for 500 ns for the 128-lipid bilayer (Figure 2E). Pore-opening PMFs are shown as dashed lines and pore-closing PMFs as solid lines. The convergence of the PMFs was further tested by computing the PMFs from simulation time blocks with increasing equilibration time, as indicated in the figure legends.

DOI: 10.1021/acs.jctc.6b00369
J. Chem. Theory Comput. 2016, 12, 3261–3269

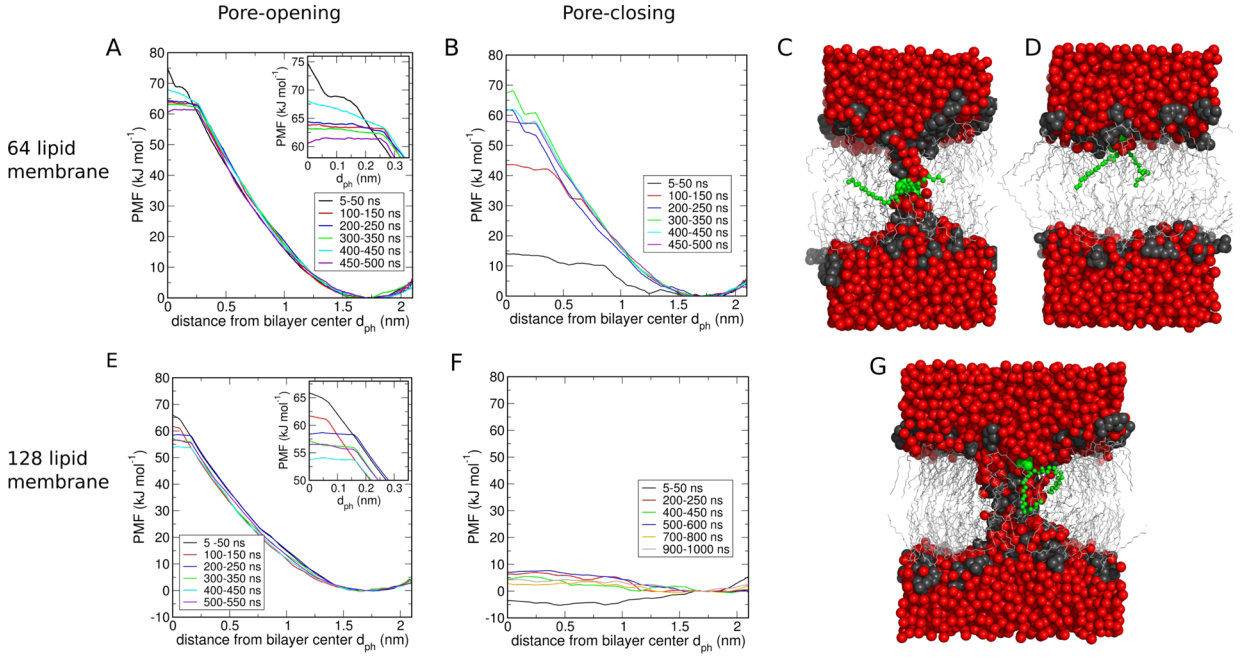

Figure 3. Pore formation using the distance of a single phosphate group from the membrane center, d_{ph}, as the reaction coordinate[36] for a membrane of (A–D) 64 or (E–G) 128 DMPC lipids. (A, E) PMFs for pore opening and (B, F) for pore closing. Pronounced hysteresis between pore opening and pore closing is observed for the 128-lipid system. (C, D) Final simulation snapshot of the 64-lipid system at (C) $d_{ph} = 0$ and (D) $d_{ph} \approx 1.2$ nm taken from the pore-closing umbrella sampling simulations, demonstrating that the pore closed within 500 ns of umbrella sampling. Lipid tails are visualized as gray sticks, headgroups as black spheres, and water atoms as red spheres. The lipid with the restrained phosphate group is highlighted in green. (G) Final snapshot of the 128-lipid membrane at $d_{ph} \approx 1.2$ nm taken from the pore-closing simulation. The pore did not close even after 1 μs of umbrella sampling.

The PMFs typically exhibit a quadratic regime at small ξ_R, corresponding to the thinning of the intact membrane and, in other words, bending of the headgroup layer toward the membrane center. The nucleation of the transmembrane pore is indicated by a kink in the PMFs. Following pore nucleation, the pore grows in size with increasing ξ_R, as reflected by a reduced slope in the PMF.

We observed pronounced hysteresis between the pore-opening and pore-closing PMFs. For instance, the pore-opening PMF computed from the 400–500 ns block of the 128-lipid system (Figure 2E, dashed magenta curve) indicates pore nucleation at $\xi_R = 0.4$ with a nucleation free energy of 115 kJ mol^{-1}. These numbers are qualitatively similar to the results for a membrane of 512 DPPC lipids under tension reported by Wohlert et al.,[30] who found pore nucleation at $\xi_R \approx 0.45$ and a nucleation energy of ~90 kJ mol^{-1}. In discrepancy to the pore-opening PMF, the corresponding pore-closing PMF suggests pore nucleation at $\xi_R = 0.3$ with a nucleation free energy of only 60 kJ mol^{-1} (Figure 2E, solid magenta curve). Hence, the simulations provide only a crude estimate of the nucleation free energy, as the converged result may be any value between 60 and 115 kJ mol^{-1}. This hysteresis indicates poor convergence of the PMFs as a result of long autocorrelation times of the pore nucleation and closing dynamics. Increasing the equilibration time in steps of 100 ns reduced the hysteresis only slightly, suggesting that at least microsecond umbrella simulations would be required to obtain converged PMFs.

To gain structural insight into the mechanisms underlying the hysteresis, we calculated the number of water molecules, N_{water}, present in a membrane-spanning cylinder centered at the pore as a function of ξ_R (see Methods). N_{water} was computed from each umbrella sampling window used for pore-opening and pore-closing PMF calculations (Figure 2B,F, black and red curves). In line with the PMFs, the N_{water} curves demonstrate pronounced hysteresis. Indeed, the curves suggest that the pore-opening and pore-closing simulations sampled similar conformations only at small or large ξ_R and highly distinct conformations at intermediate ξ_R. This finding was confirmed by visual inspection of the simulation trajectories (Figure 2C,D,G,H). At $\xi_R \approx 0.37$ during pore-opening simulations, water penetrates the membrane only partially, either in a symmetric shape (Figure 2G) or in an asymmetric shape (Figure 2C), similar to a "hanging droplet" as observed in simulations of ion permeation across membranes.[26,50,51] However, water never spans the entire membrane. In contrast, at $\xi_R \approx 0.37$ during pore-closing simulations, the simulations exhibit a fully formed water-filled pore that never closed within 500 ns (Figure 2D/H). Taken together, the pore-opening and pore-closing simulations sample different regions of phase space at intermediate ξ_R, corresponding to (i) an open, fully hydrated pore (Figure 2B,F, blue area) or (ii) a perturbed membrane *without* a fully formed pore (Figure 2B,F, green area). The simulations do not cross the transition state between these distinct regions within 500 ns of simulation (Figure 2B,F, yellow area). In addition, our analysis suggests that the transition between the open and closed pore would occur orthogonal (in phase space) to the reaction coordinate ξ_R, rationalizing why steering the system along ξ_R does not guide the system over the transition state for pore formation.

Distance of a Phosphate from the Bilayer Center, d_{ph}. Figure 3 shows the PMFs calculated using the distance of a single phosphate group from the bilayer center, d_{ph}, as the reaction coordinate for pore formation.[34,36,37] We computed PMFs for membranes of 64 DMPC lipids as reported by

DOI: 10.1021/acs.jctc.6b00369
J. Chem. Theory Comput. 2016, 12, 3261–3269

Bennett et al.[37] (Figure 3A−D) and for membranes of 128 DMPC lipids to test the effect of the membrane size on the convergence of the PMFs (Figure 3E−G). The PMFs were again computed from pore-opening (Figure 3A,E) and pore-closing simulations (Figure 3B,F), and the convergence of the PMFs was tested using an increasing equilibration time for umbrella simulations (color codes are given in the figure legends). The PMFs exhibit a quadratic regime, corresponding to the thinning of the intact membrane in the absence of a transmembrane pore. The plateau regions of the PMFs reflect states with an open, fully hydrated pore, thereby allowing the phosphate group to move along the membrane normal without energetic cost. The kinks in the PMF are again indicative of pore nucleation.

We found that PMFs for the 64-lipid membranes reported by Bennett et al.[37] converged within 500 ns of simulation time per umbrella window, as suggested by similar pore-opening and pore-closing PMFs (Figure 3A,B). Here the pore-opening PMFs converged in even shorter simulation time compared with the pore-closing PMFs. Indeed, the pore-opening PMFs hardly change with increasing equilibration time beyond 100 ns, whereas the pore-closing PMFs required 450 ns of equilibration to achieve convergence, suggesting that the d_{ph} reaction coordinate efficiently forms pores but is less efficient in closing them. Typical final snapshots from pore-closing umbrella simulations with 64 lipids are shown in Figure 3C,D.

Remarkably, in contrast to the PMFs for the 64-lipid membranes, the PMFs for the 128-lipid membrane did not converge within the accessible simulation time. The respective pore-opening PMFs again hardly changed after 200 ns (Figure 3D). However, the pore-closing PMFs (Figure 3F) are essentially flat even after 1 μs of umbrella simulations, demonstrating poor convergence due to drastic hysteresis. The flat PMFs (Figure 3F) reflect the fact that the pore did not close in any of the umbrella windows within 1 μs of simulation, even after the restrained phosphate was steered back to the equilibrium position (d_{ph} = 1.7 nm), because the simulation replaced the removed phosphate in the pore by other phosphate groups (Figure 3G). Hence, the simulations do not provide a justified estimate of the free energy of pore formation since the converged free energy may take any value between 0 and 55 kJ mol^{-1}.

Our analysis confirms that steering the system along the d_{ph} coordinate provides an efficient method to create pores in membranes.[34,36,37] However, because of slow relaxation along orthogonal degrees of freedom involving other phosphate groups and water, the d_{ph} coordinate does not allow for efficient sampling of the transition state for pore formation, leading to pronounced hysteresis between pore-opening and pore-closing simulations.

In addition, the comparison between the 64- and 128-lipid systems indicates pronounced finite-size effects, as previously reported in the context of ion permeation.[50,52] To further demonstrate these finite-size effects, we conducted 20 free simulations of the 64- and 128-lipid systems, starting from an open pore. Figure 4 presents the number of water molecules within a 14 Å slab centered at the membrane center as a function of simulation time. We found that the open pore in the 64-lipid system contains ∼23 water molecules, whereas the open pore in the 128-lipid system contains ∼53 water molecules, confirming that the pore topology strongly depends on the system size. The pores in the 64-lipid system closed with an average lifetime of 50 ns (Figure 4A). In contrast, we did not

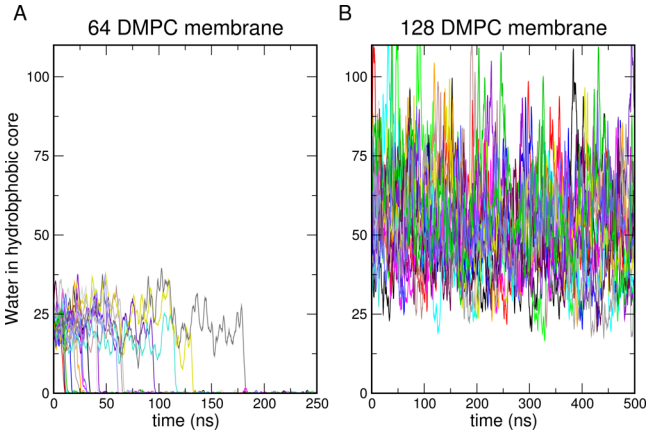

Figure 4. Free simulations of (A) 64 and (B) 128 DMPC lipids, starting from a state with an open pore. The curves show the number of water molecules within a 14 Å slab at the membrane center as a function of simulation time, taken from 20 independent 500 ns simulations. The analysis demonstrates that the pore topology and the pore-closing kinetics may be biased by finite-size effects.

observe a single pore-closing event in the 128-lipid system within a total of 10 μs of simulation (Figure 4B), suggesting that the open pore is a metastable state in the 128-lipid membrane.[13,28,29] In addition, the comparison confirms that the free energy landscape for pore formation strongly depends on the membrane size. Apparently, in the 64-lipid system, the periodic boundaries enforce stark membrane curvature in the presence of a pore (Figure 3C), thereby destabilizing the pore state and accelerating the pore-closing kinetics.

Water Density Reaction Coordinate. Figure 5 shows the PMFs using the reaction coordinate suggested by Mirjalili and Feig,[35] given by the average water density ρ_V within a membrane-spanning cylinder. In Figure 5A,D, we normalized ρ_V inside the cylinder with respect to the bulk density ρ_{bulk}, such that ρ_V/ρ_{bulk} = 1 corresponds to a fully water-filled cylinder. To test convergence and the effect of system size, PMFs were again computed from pore-opening (dashed lines) and pore-closing (solid lines) simulations using an increasing equilibration time (color codes are given in the legends) and membranes of either 128 or 256 lipids (Figure 5A,D, respectively). Similar to the PMFs presented above, these PMFs exhibit a quadratic regime reflecting the thinning of the membrane and partial penetration of water into the membrane (Figure 5C) as well as flat regions reflecting states with fully formed transmembrane pores (Figure 5B/E). The steps in nonconverged pore-closing PMFs originate from single umbrella windows in which the pores did not close within simulation time.

For the 128-lipid membrane, the PMFs converged within ∼500 ns, as demonstrated by the nearly identical pore-opening and pore-closing PMFs. The pore-opening and pore-closing simulations are also subject to hysteresis, but the hysteresis is removed within a shorter simulation time compared with the ξ_R and d_{ph} coordinates considered above. Consequently, steering the system along ρ_V is the only method used in this study that was capable of closing the transmembrane pore within 500 ns (Figure 5C).

However, the pore-opening PMFs converged with a shorter equilibration time than the pore-closing PMFs. Hence, the ρ_V coordinate, like the d_{ph} coordinate, is efficient in forming transmembrane pores but less efficient for pore closure. Visual

DOI: 10.1021/acs.jctc.6b00369
J. Chem. Theory Comput. 2016, 12, 3261−3269

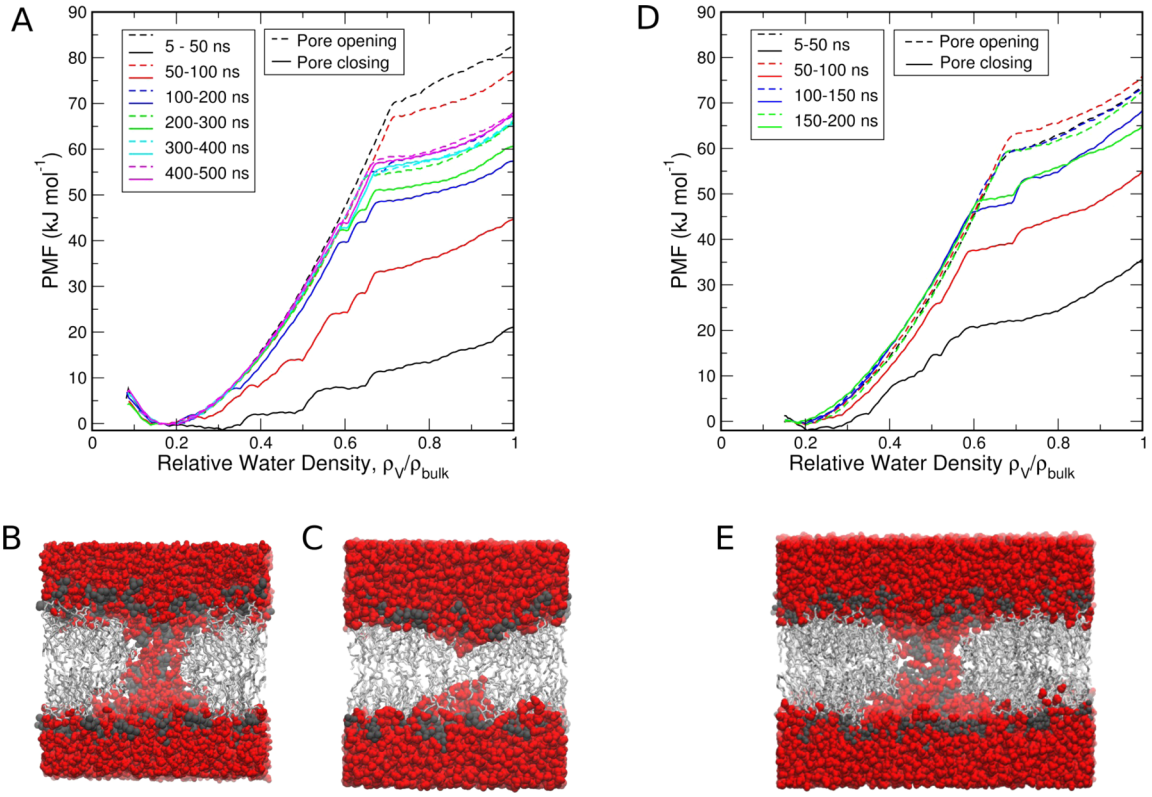

Figure 5. Pore formation using the water density inside a membrane-spanning cylinder as the reaction coordinate[35] and a membrane of (A−C) 128 or (D−F) 256 DMPC lipids. (A) PMFs for pore opening (dashed lines) and pore closing (solid lines) for a membrane of 128 DMPC lipids. (B) Simulation snapshot taken from the pore-opening umbrella simulation of $\rho_V/\rho_{bulk} \approx 0.8$ showing an open pore. (C) Simulation snapshot taken from the pore-closing umbrella simulation of $\rho_V/\rho_{bulk} \approx 0.65$ at 500 ns visualizing the closing of the pore. (D) PMFs for pore opening (dashed lines) and pore closing (solid lines) for a membrane of 256 DMPC lipids. (E) Simulation snapshot taken from the pore-opening umbrella simulation of $\rho_V/\rho_{bulk} \approx 0.8$.

inspection of the trajectories showed that when the system is steered toward smaller ρ_V, the pore does not rapidly close. Instead, the water pore moves laterally, thereby reducing the number of water molecules inside the predefined membrane-spanning cylinder.

To test for possible finite-size effects, we further computed PMFs for a 256-lipid membrane, restricting the umbrella simulations to 200 ns because of computational limitations (Figure 5D,E). These PMFs converged on a similar time scale as for the 128-lipid simulations, suggesting that the free energy landscapes for pore formation are similar in the 128- and 256-lipid systems. This analysis further suggests that simulations of pore formation in the 128-lipid membrane are not significantly affected by finite-size effects.

DISCUSSION

The simulations presented here provide atomistic insight into the mechanisms involving pore formation. For all the PMFs discussed above, we consistently observed that the formation and rupture of a continuous water column is the defining feature of the transition region. Pore closing involves (i) breaking of a continuous channel of water, (ii) removal of all of the water molecules from the membrane center, which (iii) allows the lipids at the membrane center to reduce the curvature. Eventually, the lipid headgroups diffuse out from the center of the bilayer back to the equilibrium headgroup region. The disruption of a continuous water column involves breaking of multiple hydrogen bonds between water molecules that cannot be fully compensated by alternative interactions. Hence, on the basis of our simulations and previous ones,[37] we propose that the disruption of the continuous water channel is the critical and energetically expensive event that limits the kinetics of pore closure. From a computational perspective, this suggests that accurate calculations of the energy landscape for pore formation depend on an accurate model of the hydrogen-bonding network. Hence, it remains to be tested whether coarse-grained simulations or continuum models, which use simplified models of water−water interactions, predict different free energy landscapes for pore formation compared with atomistic simulations.[53,54]

An ideal reaction coordinate should be able to keep the system close to the transition state for pore formation, which would allow multiple crossings over the transition state within a single umbrella simulation. Otherwise, it is impossible to obtain a converged free energy difference between the pore-open and pore-closed states (i.e., the free energy difference beween the green and blue areas in Figure 2B,F). Finding such reaction coordinates is often difficult. Indeed, none of the coordinates investigated here follow this ideal behavior. Instead, during umbrella simulations close to the transition state, either transitions between pore-open and pore-closed states never occurred or the transition occurred only once, similar to the sampling problems reported for simulations of membrane permeation.[32,52]

The limitations of the reaction coordinates used here are further apparent from the lack of a barrier between the pore-open and pore-closed states in the PMFs. In simulations of 128

DOI: 10.1021/acs.jctc.6b00369
J. Chem. Theory Comput. 2016, 12, 3261−3269

DMPC lipids, the pore did not close in free simulations with a total simulation time of 10 μs (Figure 4B), suggesting that pore closure is associated with a significant free energy barrier. However, none of the calculated PMFs exhibit a barrier between the pore-open and pore-closed states. Hence, the transition state was crossed orthogonal to the three reaction coordinates tested here, and the barrier was integrated out. Therefore, future efforts might focus on the development of reaction coordinates that directly probe the formation and disruption of a continuous water column. We believe that such coordinates might be capable of keeping the system closer to the transition state, thereby allowing more efficient and accurate free energy calculations of pore formation. In addition, PMFs along such coordinates may quantify the free energy barrier associated with pore closure. As soon as better reaction coordinates are available, additional insight might be obtained by computing multidimensional free energy *landscapes* of pore formation, complementary to the one-dimensional PMFs considered here.

The PMF calculations along the three reaction coordinates for pore formation studied here exhibit significant differences in terms of both the resulting PMFs and the convergence. We observed that the reaction coordinates acting via perturbation of lipids suffer from stronger hysteresis and convergence issues than the coordinate acting on the water molecules. Using the water density reaction coordinate, in contrast, we achieved converged PMFs within 500 ns for both pore-opening and pore-closing simulations. Nevertheless, all three reaction coordinates suffer from hysteresis due to slow relaxation along degrees of freedom that are orthogonal to the reaction coordinate. (i) The collective radial coordinate, ξ_R, steers the lipids purely in the radial direction.[30] Hence, it does not guide the lipid headgroups and/or water molecules in and out of the membrane center, as required for pore formation and closure. In addition, estimates of the pore nucleation free energy from the ξ_R coordinate are larger than the estimates from the other two coordinates. This may indicate that the ξ_R coordinate perturbs the membrane more strongly than is strictly required for pore formation. We note that these findings may depend upon the parameter ζ, which we have not tested in this study. (ii) Steering the distance of a single phosphate group from the membrane center, d_{ph}, efficiently induces pores.[34,36,37] However, it is inefficient for pore closure because the restrained phosphate can be replaced by other phosphate groups. (iii) Likewise, the water density coordinate ρ_V efficiently induces pores.[35] However, instead of closing the pore, the system can reduce ρ_V by shifting the intact water pore laterally out of the cylinder, leading to pore closure with a delay of a few hundred nanoseconds.

In addition to the influence of the reaction coordinates, we tested the role of system size in simulations of pore formation. We found increased rates of pore closure in membranes of 64 lipids compared with membranes of 128 lipids, suggesting that the barrier for pore closure is reduced by periodic boundary effects in small systems. These findings may be rationalized by the strong membrane curvature observed in such simulations with an open pore. For PMF calculations along the ρ_V coordinate, we did not find significant differences between simulations containing 128 or 256 lipids. Hence, for the simulations of small water defects considered here, membranes of 128 lipids might provide a reasonable balance between accuracy and simulation efficiency.

In this study, we have focused on the PMFs for pore formation. Since PMFs are an ensemble (or equilibrium) property, any hysteresis between pore-opening and pore-closing PMFs indicates a severe sampling problem, presumably as a consequence of using a poor reaction coordinate. In contrast, under experimental conditions, pore opening and closing are typically driven by an external perturbation, such as a transmembrane potential, which may shift the free energy minimum between the open and closed states. The pathways for pore opening and closing under such nonequilibrium conditions may very well exhibit pronounced hysteresis, as is common for first-order phase transitions, and the pathways may depend on the magnitude of the external perturbation. Hence, in a future study, it will be interesting to compute the influence of external perturbations on the free energy landscape and to compare the landscape with the actual pathways of pore opening and closing.

Finally, we note that the nucleation free energies for DMPC membranes reported by Bennett et al.[37] are slightly smaller than the values found here, despite the fact that the same force field was applied. We found that these differences might be explained by (i) the type of temperature coupling scheme and (ii) the amount of water present in the simulations (data not shown). However, these tested parameters had no influence on the hysteresis, convergence, and finite-size effects observed for the pore-opening and pore-closing simulations as described above.

CONCLUSIONS

The simulations shown here suggest that the transition state for pore formation is characterized by the formation and disruption of a continuous channel of water. We systematically compared three reaction coordinates for transmembrane pore formation and found that all three reaction coordinates efficiently form pores. However, we observed pronounced hysteresis between pore-opening and pore-closing simulations, as none of the three reaction coordinates restrain the membranes close to the transition state for pore formation. We have described the molecular mechanisms underlying the hysteresis. Hence, our study provides molecular insight into membrane defects, and it may guide ongoing efforts for the development of efficient reaction coordinates for transmembrane pore formation.

AUTHOR INFORMATION

Corresponding Authors

*E-mail: nawasth@gwdg.de.

*E-mail: jhub@gwdg.de. Phone: +49 (0)551 39 14296. Fax: +49 (0)551 39 14082.

Funding

N.A. was supported by the Dorothea Schlözer Programme of Georg-August-Universät Göttingen. We further acknowledge the financial support from the Deutsche Forschungsgemeinschaft (SFB 803/A12 and HU 1971-1/1).

Notes

The authors declare no competing financial interest.

ACKNOWLEDGMENTS

We thank Drew Bennett for sharing the simulation system and parameters of the DMPC membrane system and for insightful discussions. We also thank Marcus Mueller and Micheal Feig for discussions.

DOI: 10.1021/acs.jctc.6b00369
J. Chem. Theory Comput. 2016, 12, 3261−3269

REFERENCES

(1) Jahn, R.; Lang, T.; Südhof, T. C. *Cell* **2003**, *112*, 519−533.
(2) Fuhrmans, M.; Marelli, G.; Smirnova, Y. G.; Müller, M. *Chem. Phys. Lipids* **2015**, *185*, 109−128.
(3) Bennett, W. D.; Tieleman, D. P. *Acc. Chem. Res.* **2014**, *47*, 2244−2251.
(4) Vorobyov, I.; Olson, T. E.; Kim, J. H.; Koeppe, R. E.; Andersen, O. S.; Allen, T. W. *Biophys. J.* **2014**, *106*, 586−597.
(5) LaRocca, T.; Stivison, E.; Mal-Sarkar, T.; Hooven, T.; Hod, E.; Spitalnik, S.; Ratner, A. *Cell Death Dis.* **2015**, *6*, e1773.
(6) Lenertz, L. Y.; Gavala, M. L.; Hill, L. M.; Bertics, P. J. *Purinergic Signalling* **2009**, *5*, 175−187.
(7) Kägi, D.; Ledermann, B.; Bürki, K.; Seiler, P.; Odermatt, B.; Olsen, K. J.; Podack, E. R.; Zinkernagel, R. M.; Hengartner, H. *Nature* **1994**, *369*, 31−37.
(8) Law, R. H.; Lukoyanova, N.; Voskoboinik, I.; Caradoc-Davies, T. T.; Baran, K.; Dunstone, M. A.; D'Angelo, M. E.; Orlova, E. V.; Coulibaly, F.; Verschoor, S.; Browne, K. A.; Ciccone, A.; Kuiper, M. J.; Bird, P. I.; Trapani, J. A.; Saibil, H. R.; Whisstock, J. C. *Nature* **2010**, *468*, 447−451.
(9) Brogden, K. A. *Nat. Rev. Microbiol.* **2005**, *3*, 238−250.
(10) Bechara, C.; Sagan, S. *FEBS Lett.* **2013**, *587*, 1693−1702.
(11) Zhelev, D. V.; Needham, D. *Biochim. Biophys. Acta, Biomembr.* **1993**, *1147*, 89−104.
(12) Akinlaja, J.; Sachs, F. *Biophys. J.* **1998**, *75*, 247−254.
(13) Melikov, K. C.; Frolov, V. A.; Shcherbakov, A.; Samsonov, A. V.; Chizmadzhev, Y. A.; Chernomordik, L. V. *Biophys. J.* **2001**, *80*, 1829−1836.
(14) Tekle, E.; Astumian, R.; Friauf, W.; Chock, P. *Biophys. J.* **2001**, *81*, 960−968.
(15) Marrink, S.; Jähnig, F.; Berendsen, H. *Biophys. J.* **1996**, *71*, 632.
(16) Gurtovenko, A. A.; Anwar, J.; Vattulainen, I. *Chem. Rev.* **2010**, *110*, 6077−6103.
(17) Tieleman, D. P.; Leontiadou, H.; Mark, A. E.; Marrink, S.-J. *J. Am. Chem. Soc.* **2003**, *125*, 6382−6383.
(18) Leontiadou, H.; Mark, A. E.; Marrink, S. J. *Biophys. J.* **2004**, *86*, 2156−2164.
(19) Tarek, M. *Biophys. J.* **2005**, *88*, 4045−4053.
(20) Gurtovenko, A. A.; Vattulainen, I. *J. Am. Chem. Soc.* **2005**, *127*, 17570−17571.
(21) Böckmann, R. A.; De Groot, B. L.; Kakorin, S.; Neumann, E.; Grubmüller, H. *Biophys. J.* **2008**, *95*, 1837−1850.
(22) Leontiadou, H.; Mark, A. E.; Marrink, S. J. *J. Am. Chem. Soc.* **2006**, *128*, 12156−12161.
(23) Sengupta, D.; Leontiadou, H.; Mark, A. E.; Marrink, S.-J. *Biochim. Biophys. Acta, Biomembr.* **2008**, *1778*, 2308−2317.
(24) Herce, H.; Garcia, A.; Litt, J.; Kane, R.; Martin, P.; Enrique, N.; Rebolledo, A.; Milesi, V. *Biophys. J.* **2009**, *97*, 1917−1925.
(25) Tepper, H. L.; Voth, G. A. *Biophys. J.* **2005**, *88*, 3095−3108.
(26) Neale, C.; Madill, C.; Rauscher, S.; Pomès, R. *J. Chem. Theory Comput.* **2013**, *9*, 3686−3703.
(27) Marrink, S.-J.; Lindahl, E.; Edholm, O.; Mark, A. E. *J. Am. Chem. Soc.* **2001**, *123*, 8638−8639.
(28) Abiror, I.; Arakelyan, V.; Chernomordik, L.; Chizmadzhev, Y. A.; Pastushenko, V.; Tarasevich, M. *Bioelectrochem. Bioenerg.* **1979**, *6*, 37−52.
(29) Evans, E.; Heinrich, V.; Ludwig, F.; Rawicz, W. *Biophys. J.* **2003**, *85*, 2342−2350.
(30) Wohlert, J.; den Otter, W. K.; Edholm, O.; Briels, W. J. *J. Chem. Phys.* **2006**, *124*, 154905.
(31) Torrie, G. M.; Valleau, J. P. *Chem. Phys. Lett.* **1974**, *28*, 578−581.
(32) Neale, C.; Pomès, R. *Biochim. Biophys. Acta, Biomembr.* **2016**, DOI: 10.1016/j.bbamem.2016.03.006.
(33) Tolpekina, T.; Den Otter, W.; Briels, W. *J. Chem. Phys.* **2004**, *121*, 12060−12066.
(34) Sapay, N.; Bennett, W. F. D.; Tieleman, D. P. *Soft Matter* **2009**, *5*, 3295−3302.
(35) Mirjalili, V.; Feig, M. *J. Chem. Theory Comput.* **2015**, *11*, 343−350.
(36) Tieleman, D. P.; Marrink, S.-J. *J. Am. Chem. Soc.* **2006**, *128*, 12462−12467.
(37) Bennett, W. F. D.; Sapay, N.; Tieleman, D. P. *Biophys. J.* **2014**, *106*, 210−219.
(38) Berger, O.; Edholm, O.; Jahnig, F. *Biophys. J.* **1997**, *72*, 2002−2013.
(39) Berendsen, H. J. C.; Postma, J. P. M.; van Gunsteren, W. F.; Hermans, J. In *Intermolecular Forces*; Pullman, B., Ed.; Reidel: Dordrecht, The Netherlands, 1981; pp 331−342.
(40) Hess, B.; Kutzner, C.; van der Spoel, D.; Lindahl, E. *J. Chem. Theory Comput.* **2008**, *4*, 435−447.
(41) Miyamoto, S.; Kollman, P. A. *J. Comput. Chem.* **1992**, *13*, 952−962.
(42) Hess, B.; Bekker, H.; Berendsen, H. J. C.; Fraaije, J. G. E. M. *J. Comput. Chem.* **1997**, *18*, 1463−1472.
(43) van Gunsteren, W. F.; Berendsen, H. J. C. *Mol. Simul.* **1988**, *1*, 173−185.
(44) Berendsen, H. J. C.; Postma, J. P. M.; van Gunsteren, W. F.; DiNola, A.; Haak, J. R. *J. Chem. Phys.* **1984**, *81*, 3684−3690.
(45) Darden, T.; York, D.; Pedersen, L. *J. Chem. Phys.* **1993**, *98*, 10089−10092.
(46) Essmann, U.; Perera, L.; Berkowitz, M. L.; Darden, T.; Lee, H.; Pedersen, L. G. *J. Chem. Phys.* **1995**, *103*, 8577−8592.
(47) Kumar, S.; Bouzida, D.; Swendsen, R. H.; Kollman, P. A.; Rosenberg, J. M. *J. Comput. Chem.* **1992**, *13*, 1011−1021.
(48) Hub, J. S.; de Groot, B. L.; van der Spoel, D. *J. Chem. Theory Comput.* **2010**, *6*, 3713−3720.
(49) Hess, B. *J. Chem. Phys.* **2002**, *116*, 209−217.
(50) Hu, Y.; Ou, S.; Patel, S. *J. Phys. Chem. B* **2013**, *117*, 11641−11653.
(51) Cardenas, A. E.; Shrestha, R.; Webb, L. J.; Elber, R. *J. Phys. Chem. B* **2015**, *119*, 6412−6420.
(52) Wang, Y.; Hu, D.; Wei, D. *J. Chem. Theory Comput.* **2014**, *10*, 1717−1726.
(53) Ting, C. L.; Appelö, D.; Wang, Z.-G *Phys. Rev. Lett.* **2011**, *106*, 168101.
(54) Bennett, W. D.; Tieleman, D. P. *J. Chem. Theory Comput.* **2011**, *7*, 2981−2988.

DOI: 10.1021/acs.jctc.6b00369
J. Chem. Theory Comput. 2016, 12, 3261−3269